Constructal conjugate cooling channels with internal heat generation

O.T. Olakoyejo, T. Bello-Ochende *, J.P. Meyer

Department of Mechanical and Aeronautical Engineering, University of Pretoria, Pretoria Private Bag X20, Hatfield 0028, South Africa

ARTICLE INFO

ABSTRACT

This paper presents a geometric optimisation of conjugate cooling channels in forced convection with internal heat generation. Two configurations were studied; circular channels and square channels. The configurations were optimised in such a way that the peak temperatures were minimised subject to the constraint of fixed total global volume. The fluid was forced through the cooling channels by the pressure difference across the channels. The structure has one degree of freedom as design variable: channel hydraulic diameter and once the optimal channel hydraulic diameter is found, optimal elemental volume and channel-to-channel spacing result. A gradient-based optimisation algorithm is applied in order to search for the best and optimal geometric configurations that improve thermal performance by minimising thermal resistance for a wide range of dimensionless pressure difference. This optimiser adequately handles the numerical objective function obtained from CFD simulations. The results obtained show the behaviour of the applied pressure difference on the optimised geometry. There are unique optimal design variables for a given pressure difference. The numerical results obtained are in agreement with the theoretical formulation using scale analysis and method of intersection of asymptotes.

© 2012 Elsevier Ltd. All rights reserved.

1. Introduction

A procedure that sufficiently allocates and optimises a fixed global space constraint using a physical law for heat-generating devices has been adopted recently as an optimisation technique [1]. The method seeks to optimise the flow architecture, which predicts the flow and thermal fluid behaviour in a structure that is subject to a global volume constraint. This body of knowledge is called constructal theory and design. Bejan [1] stated this law as: *For a finite-size system to persist in time* (*to live*), *it must evolve in such a way that it provides easier access to the imposed* (*global*) *currents that flow through it*. The application of this theory started with Bejan and Sciubba [2], who obtained a dimensionless pressure difference number for optimal spacing of an array of parallel plates and a maximum heat transfer density, which can be fitted into a fixed volume in an electronic cooling application using the method of intersection of asymptotes.

The applications of this theory have been reviewed most recently by the work of Bejan and Lorente [3] in which it was concluded that, under certain constraints, the best architecture of a flow system can be achieved by the one that gives less flow resistances, or allows high flow access. In other words, the shapes of the channels and elemental structure that are subject to global constraint are allowed to morph. The optimisation of heat exchanger

and multiscale devices by constructal theory has also recently been reviewed and summarised by Reis [4] and Fan and Luo [5].

Yilmaz et al. [6] studied the optimum shape and dimensions for convective heat transfer of laminar flow at constant wall temperatures for ducts with parallel plate, circular, square and equilateral triangle geometries. Approximate equations were derived in the form of maximum dimensionless heat flux and optimum dimensionless hydraulic diameter in terms of the duct shape factors and the Prandlt number (Pr).

Muzychka [7] used this theory and Bejan's intersection of asymptotes method to present an analytical optimisation of circular and non-circular cooling channel geometries. Also, he has recently studied and analysed the optimisation of microtube heat sinks and heat exchangers for maximum thermal heat transfer by using a multiscale design approach [8]. In his analysis, he was able to show that through the use of interstitial microtubes, the maximum heat transfer rate density for an array of circular tubes increased. He obtained an approximate solution using Bejan's intersection of asymptotes method. The multiscale design approach gives a greater thermal performance of heat exchanger and heat sink compared with the conventional design methods.

Da Silva et al. [9] optimised the space allocation on a wall occupied by discrete heat sources with a given heat generation rate by forced convection using the constructal design in order to minimise the temperature of the hot spot on the wall. Bejan and Fautrelle [10], maximised the heat transfer density in a multiscale structure filled by multiple length scale plates that generate heat.

* Corresponding author. Tel.: +27 12 4203105; fax: +27 12 362 5124.
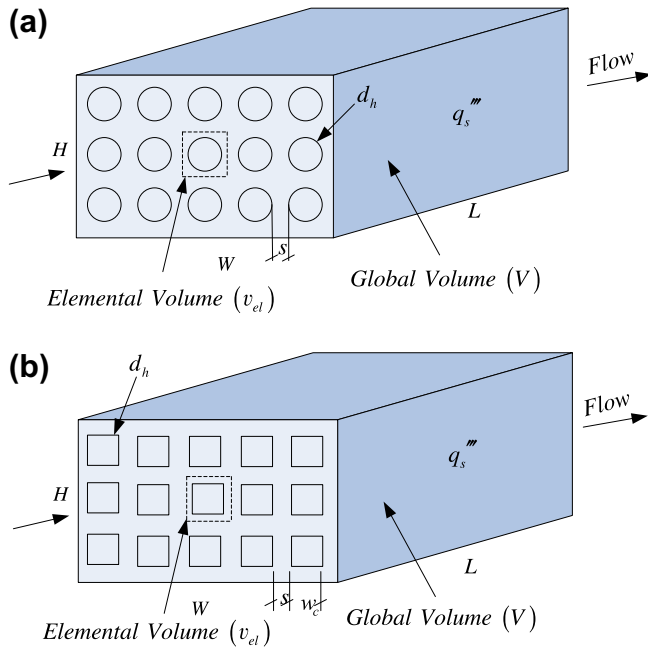 E-mail address: tunde.bello-ochende@up.ac.za (T. Bello-Ochende).

Nomenclature

A_c	cross sectional area of the channel, m^2		W	structure width, m
A_s	cross sectional area of the structure, m^2		w	elemental width, m
Be	Bejan number		x, y, z	cartesian coordinates, m
C_P	specific heat at constant pressure, J/kg K			
Cyl	cylindrical configuration		*Greek symbols*	
d_h	hydraulic diameter, m		α	thermal diffusivity, m^2/s
H	structure height, m		μ	viscosity, kg/m.s
h	elemental height , m		v	kinematics viscosity, m^2/s
i	mesh iteration index		ρ	density, kg/m^3
k	thermal conductivity, W/mK		∂	differential
L	axial length, m		∞	far extreme end, free stream
N	number of channels		φ	porosity
n	normal		$\varDelta$	difference
P	pressure, kPa		∇	differential operator
P_c	perimeter of the channel		τ	shear stress, Pa
P_o	Poiseuille number		γ	convergence criterion
Pr	Prandtl number			
$\dot{q}''$	heat flux, W/m^2		*Subscripts*	
q_s'''	internal heat generation density, W/m^3		$\sim$	dimensionless
$\dot{q}$	heat transfer rate, W		c	channel
R	thermal resistance		f	fluid
Re	Reynolds number		in	inlet
s	channel spacing, m		l	large
Sqr	square configuration		max	maximum, peak
T	temperature, ^{0}C		min	minimum
$\tilde{T}_{\max}$	dimensionless maximum temperature $\left(\tilde{T}_{\max} = \frac{T-T_{\text{in}}}{q''' v^{2/3}/k_f}\right)$		opt	optimum
$\vec{u}$	velocity vector, m/s		s	solid
V	global structure volume, m^3		sm	small
v_c	channel volume, m^3		w	wall
v_{el}	elemental volume, m^3			

They inserted additional parallel plates and optimised the spacing in the flow structure.

Bello-Ochende and Bejan [11] studied and extended the work of Bejan and Fautrelle [10] numerically based on the concept of constructal theory. Also, Bello-Ochende et al. [12,13] studied a three-dimensional optimsation of heat sink and cooling channels with heat flux using scale analysis and the intersection of asymptotes method based on constructal theory to investigate and predict the design and optimisation of the geometric configurations of the cooling channels.

Matos et al. [14] conducted three-dimensional numerical and experimental analyses of laminar rows of tubes. Ordonez [15] conducted a two-dimensional heat transfer analysis in a heat-generated volume with cylindrical cooling channels and air as the working fluid. Reis et al. [16] optimised the internal configurations of parallel plate and cylindrical channels using constructal theory to understand the morphology of particle agglomeration and the design of air-cleaning devices.

Also, the constructal theory for optimisation of several components and systems and components in engineering applications has been extensively discussed and documented in the literature [17–19].

This paper focuses on the study of three-dimensional laminar forced convection cooling of solid structures. It examines the optimisation of a fixed and finite global volume of solid materials for two cooling channel configurations (circular and square channels) with a uniform internal heat generation rate. This was achieved by varying and arranging the elemental volume of structure with cooling channels of fixed porosity to reduce the peak temperature at any point inside the global volume. The design variables were dealt with simultaneously since the effect of one of the design variables cannot be neglected, especially at a microscopic scale. Bau [20] suggested that the "integrity of fin thickness (channel spacing) during fabrication and operation should be asserted and maintained". Therefore, the need exists to consider the three design variables simultaneously. It is expected that there must be an optimal configuration that gives the minimum peak temperature. Any values below or above those of the optima design variables will cause the working fluid to not be properly used, which will cause the peak temperature to increase and will lead to thermal stress that affects the performance of cooling channels.

2. Models

The physical configuration is shown schematically in Fig. 1. The system consists of parallel cooling channels of length, L of fixed global volume, V for the two configurations. The internal heat generation in the solid material is q_s'''. An elemental volume, v_{el}, consisting of a cooling channel and the surrounding solid was used for analysis because of the assumption of the symmetrical heat distribution inside the structure. However, the elemental volume v_{el} is not fixed and is allowed to morph by varying cooling channel shape v_c for fixed porosity and fixed channel length. The heat transfer in the elemental volume is a conjugate problem, which combines heat conduction in the solid and the convection in the working fluid. These two modes of heat transfer are coupled together through the continuity of heat flux at the solid-fluid interface.

2.1. Design variables

In Fig. 2, an elemental volume, v_{el}, constraint is considered to be composed of an elemental cooling channel of hydraulic diameter,

Fig. 1. Ducts with cooling channels: (a) circular cooling channels. (b) square cooling channel.

d_h, and the surrounding solid of thickness s (spacing between channels) and these variables are defined as:

$$w = h \quad (1)$$

$$v_{el} = w^2 L \quad (2)$$

$$w = d_h + s \quad (3)$$

For a fixed length of the channel, we have

$$A_s = HW \quad (4)$$

Therefore, the total number of channels in the structure arrangement can be defined as:

$$N = \frac{HW}{(d_h + s)^2} \quad (5)$$

However, the void fraction or porosity of the unit structure can be defined [15] as:

$$\phi = \frac{v_c}{v_{el}} \approx \left(\frac{d_h}{w}\right)^2 \quad (6)$$

The fundamental problem under consideration is the numerical optimisation of the hydraulic diameter, d_h, and spacing between channels, s, which corresponds to the minimum resistance of a fixed volume for a given pressure drop. The optimisation is evaluated from the analysis of the extreme limits of $(0 \leqslant v_{el} \leqslant \infty)$, $(0 \leqslant d_h \leqslant \infty)$ and the extreme limits of $(0 \leqslant s \leqslant \infty)$. The optimal values of the design variables within the prescribed interval of the extreme limits exhibit the minimum thermal resistance.

The temperature distribution in the model was determined by solving the equation for the conservation of mass, momentum and energy numerically. The discretised three-dimensional
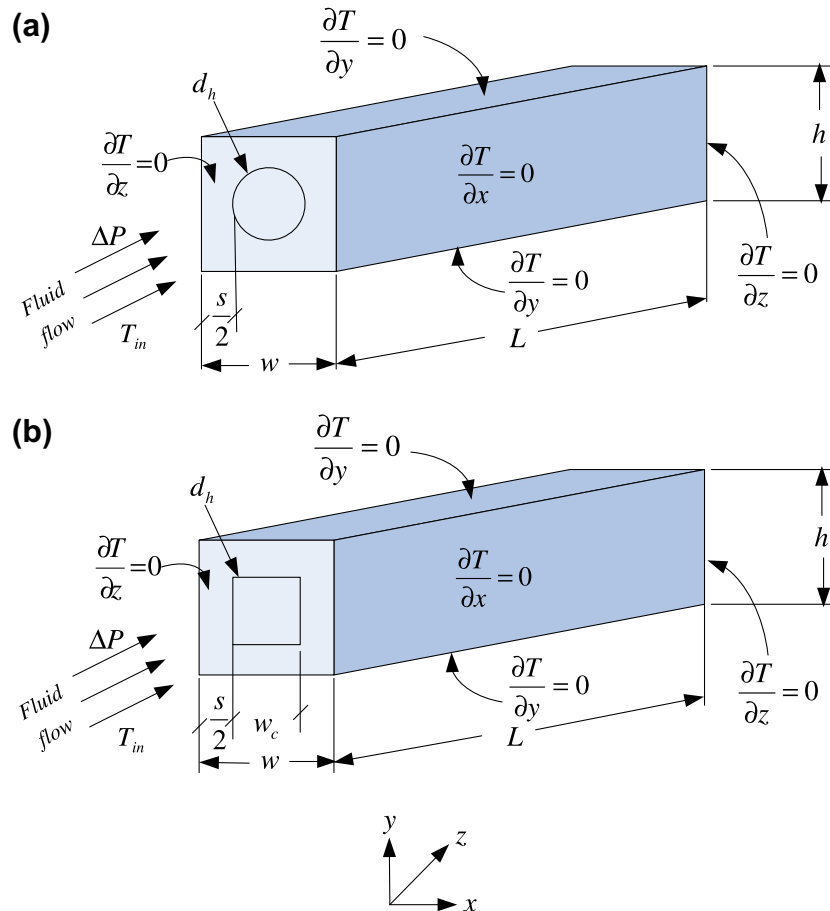
Fig. 2. The boundary conditions of the three-dimensional computational domain of the cooling channel: (a) cylinder, (b) square.
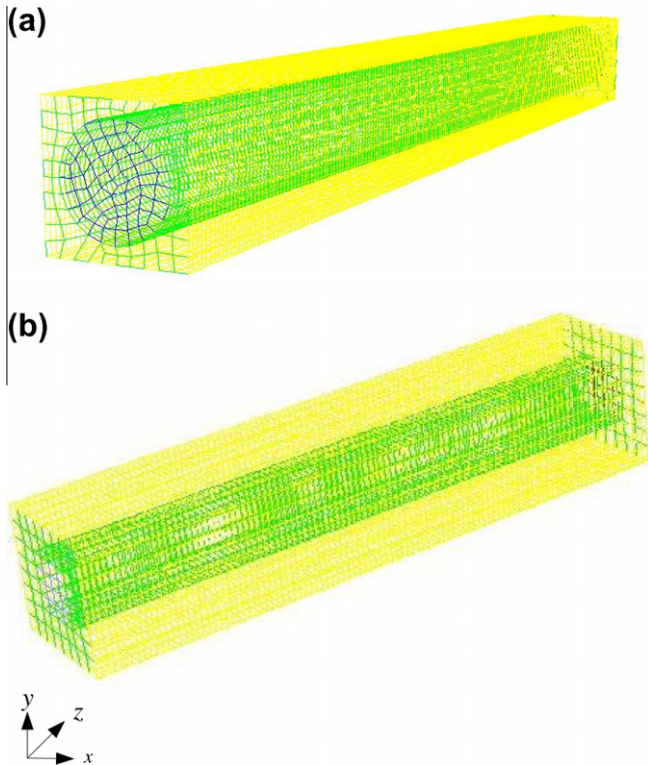
Fig. 3. The discretised 3-D computational domain: (a) cylinder, (b) square.

computational domains of the circular and square configurations are shown in Fig. 3. The cooling fluid was water; it is assumed to be in single-phase, steady, and a Newtonian fluid with constant thermophysical properties, and was forced through the cooling channels by a specified pressure difference, ΔP, across the axial length of the structure. Water is more promising than air, because air-cooling techniques are not likely to meet the challenge of high heat dissipation in electronic packages [21,22]. The governing differential equations used for the fluid flow and heat transfer analysis inside the unit volume of the structure are:

$$\nabla \cdot \vec{u} = 0 \tag{7}$$

$$\rho(\vec{u} \cdot \nabla \vec{u}) = -\nabla P + \mu \nabla^2 \vec{u} \tag{8}$$

$$\rho_f C_{Pf}(\vec{u} \cdot \nabla T) = k_f \nabla^2 T \tag{9}$$

while the energy equation for a solid with internal heat generation is given as:

$$k_s \nabla^2 T + q_s''' = 0 \tag{10}$$

The continuity of the heat flux at the interface between the solid and the liquid is given as:

$$k_s \frac{\partial T}{\partial n}\bigg| = k_f \frac{\partial T}{\partial n}\bigg| \tag{11}$$

A no-slip boundary condition is specified at the wall of the channel,

$$\vec{u} = 0 \tag{12}$$

and at the inlet ($x = 0$)

$$u_x = u_y = 0 \tag{13}$$

$$T = T_{in} \tag{14}$$

$$P = \frac{Be\alpha\mu}{L^2} + P_{out} \tag{15}$$

where, Be is the dimensionless pressure difference called the Bejan number [23,24].

At the channel outlet ($x = L$), a zero normal stress is prescribed, and

$$P_{out} = 1 \text{ atm} \tag{16}$$

At the solid boundaries, all the outside walls and plane of symmetry of the solid structure were modelled as adiabatic as shown in Fig. 2. That is:

$$\nabla T = 0 \tag{17}$$

and an internal heat generation, q_s''', is assumed in the solid material.

The measure of performance is the minimum global thermal resistance, which could be expressed in a dimensionless form as:

$$R_{min} = \frac{k_f(T_{max} - T_{in})_{min}}{q_s''' L^2} \tag{18}$$

and it is a function of the optimised design variables and the peak temperature,

$$R_{min} = f(d_{h_{opt}}, s_{opt}, v_{el_{opt}}, N_{opt}, T_{max_{min}}) \tag{19}$$

where R_{min} is the minimised dimensionless thermal resistance for the optimised design variables. The inverse of R_{min} is the maximised overall global thermal conductance.

3. Numerical procedure and grid analysis

The simulation procedure began by fixing the length of the channel, applied pressure difference, porosity, internal heat generation and material properties and we kept varying the values of elemental volume and hydraulic diameter of the channel in order to identify the best (optimal) internal and external geometries that minimised the peak temperature.

The numerical solution of the continuity, momentum and energy Eqs. (7)–(10) along with the boundary conditions (11)–(17) was obtained by using a three-dimensional commercial package FLUENT™ [25], which employs a finite volume method. The details of the method were explained by Patankar [26]. The computational fluid dynamics package was coupled with the geometry and mesh generation package GAMBIT [27] using MATLAB [28] to allow the automation and running of the simulation process. After the simulation converged, an output file was obtained containing all the necessary simulation data and results for the post-processing and analysis. The computational domain was discretised using hexahedral/wedge elements. A second-order upwind scheme was used to discretise the combined convection and diffusion terms in the momentum and energy equations. The SIMPLE algorithm was then employed to solve the coupled pressure-velocity fields of the transport equations. A flow chart representing the numerical procedure is shown in Fig. 4. The solution is assumed to be converged when the normalised residuals of the mass and momentum equations fall below 10^{-6} and while the residual convergence of energy equation was set to less than 10^{-10}. The number of grid cells used for the simulations varied for different elemental volume and porosities. However, grid independence tests for several mesh refinements were carried out to ensure the accuracy of the numerical results. The convergence criterion for the overall thermal resistance as the quantity monitored is:

$$\gamma = \frac{|(T_{max})_i - (T_{max})_{i-1}|}{|(T_{max})_i|} \leqslant 0.01 \tag{20}$$

where i is the mesh iteration index. The mesh is more refined as i increases. The $i-1$ mesh is selected as a converged mesh when the criterion Eq. (20) is satisfied.
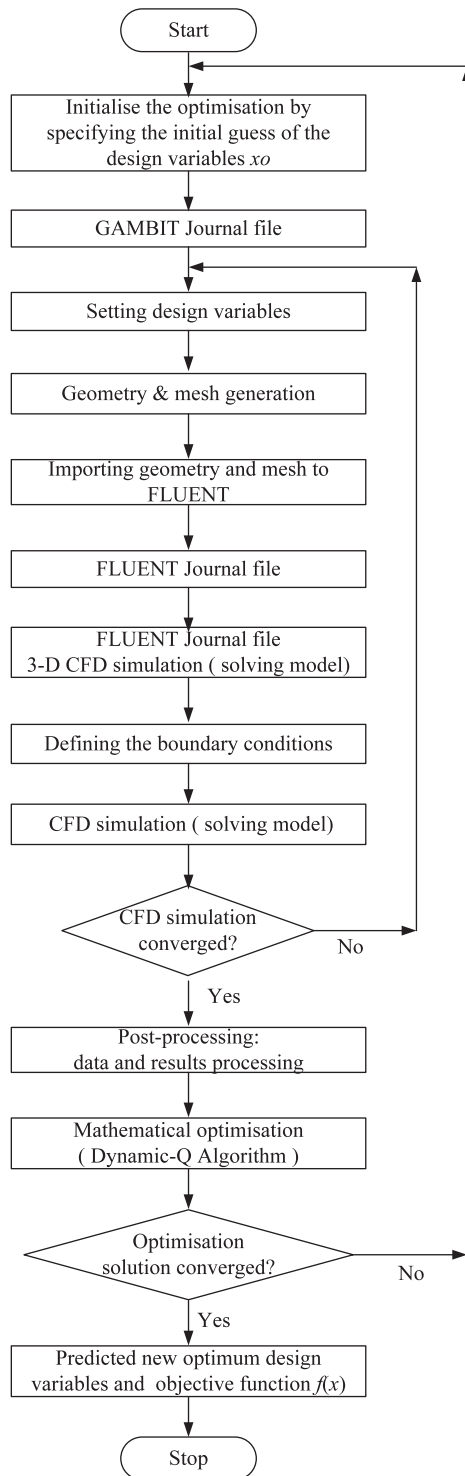
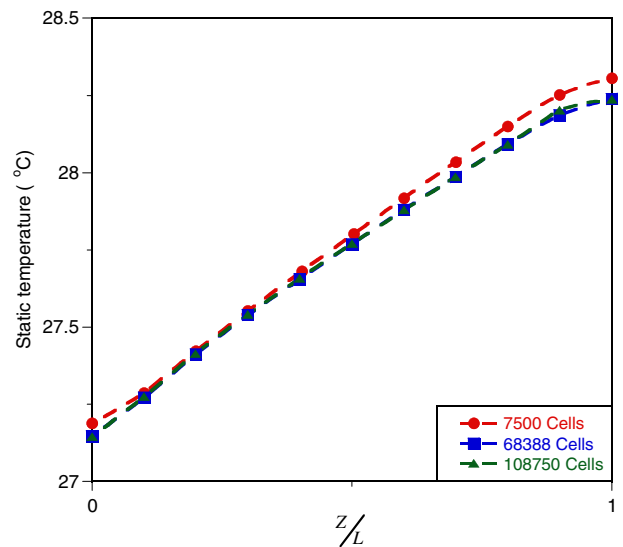Fig. 4. Flow chart of numerical simulation.

Fig. 5. Grid independent test for cylindrical configuration at fixed pressure difference and porosity.

the internal heat generation within the solid was taken to be fixed at 100 kW/cm^3. The thermophysical properties of water [29] used in this study were based on water at 300 K and the inlet water temperature was fixed at this temperature.

Fig. 5 shows the grid independence test for a cylindrical configuration for v_{el} = 0.4 mm^3 and φ = 0.2 for ΔP = 50 kPa. Also, computational cells of 7500, 68 388 and 108 750 were used for the grid independence test. It is observed that an almost identical results were predicted when 68 388 and 108 750 cells were used. Therefore, a further increase in the cell density beyond 68 388 has a negligible effect on the numerical result.

The validation of the numerical simulation was also carried out by comparing the present simulation for a circular configuration with the dimensionless temperature simulation of Ordonez [15] as shown in Fig. 6. The curves were found to be similar in trend and the optimised hydraulic diameters were also found to be in good agreement.

Figs. 7–10 show the existence of an optimum hydraulic diameter and spacing of the cooling channel and elemental volume structure, respectively, where the peak temperature is minimised at any point in the channel for the two configurations studied. These Figures are for the case where the pressure difference was fixed at ΔP = 50 kPa for 0.025 mm^3 ⩽ v_{el} ⩽ 5 mm^3 and 0.1 ⩽ φ ⩽ 0.2.

Fig. 7 shows the graph of peak temperature as a function of the channel hydraulic diameter. It shows that there exists an optimal channel hydraulic diameter, which lies in the range of 50 μm ⩽ d_h ⩽ 220 μm, minimising the peak temperature. The channel spacing also has a strong effect on the peak temperature, as shown in Fig. 8. The minimum peak temperature is achieved when the optimal channel spacing exists in the range of 50 μm ⩽ s ⩽ 350 μm. These indicate that the peak temperature decreases as global design variables increase and that maxima (optimal) values of the design variables are reached beyond which the peak temperature begins to increase. Therefore, the global peak temperature decreases as the design variables increase or the global peak temperature decreases as the design variables decrease until it gets to the optimal design values. Any increase or decrease in the design variable beyond the optimal values indicates that the working fluid is not properly engaged in the cooling process, which is detrimental to the global performance of the system.

Also, in Fig. 9, there exists an optimal elemental volume of the structure that minimised the peak temperature and this lies in the

4. Numerical results using a traditional method

In this section, the numerical results are presented using a traditional method by post-processing the simulation data and results manually. The elemental volume of the structure was in the range of 0.025 mm^3 to 5 mm^3 and the porosities ranged between 0.1 ⩽ φ ⩽ 0.2 and a fixed length of L = 10 mm at a fixed pressure drop of ΔP = 50 kPa. The global structure is assume to have a total global cross-sectional area of 2.5 mm by 2.5 mm. The thermal conductivity of the solid structure (silicon) was 148 W/m K; and

Fig. 6. Thermal resistance curves: present study and Ordonez [16].

Fig. 8. Effect of optimised channel spacing, s, on the peak temperature.

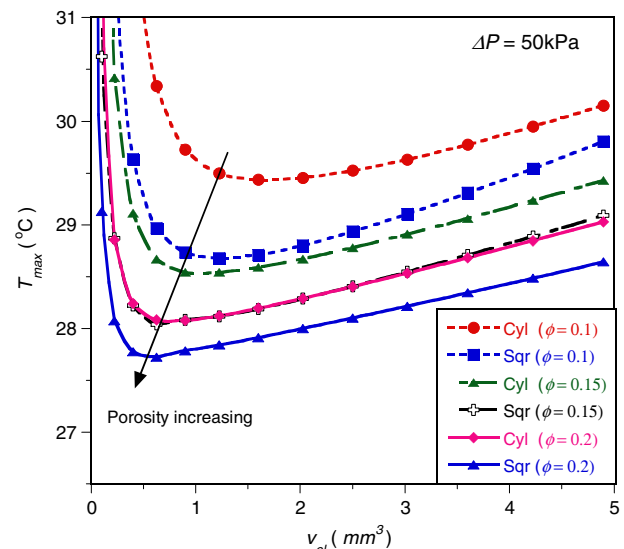**Fig. 7.** Effect of optimised hydraulic diameter d_h, on the peak temperature.

Fig. 9. Effect of optimised elemental volume, v_{el}, on the peak temperature.

range of $0.2 \text{ mm}^3 \leqslant v_{el} \leqslant 2 \text{ mm}^3$. The results show that the optimal arrangement of the elemental volume for the entire structure at this fixed pressure difference should be very small in order to achieve better cooling.

Fig. 10 shows existence of an optimal total number of channels required in the structure that minimised the peak temperature and this also, lies in the range of $10 \leqslant N \leqslant 120$.

It can also be shown from Figs. 7 and 10 that porosity has a significant effect on the peak temperature and the overall thermal resistance. There is no optimum porosity. The best performance occurs at the highest porosity, which means as the porosity increases, the peak temperature decreases.

5. Mathematical optimisation (Dynamic-Q)

The results shown in the preceding session were done using a traditional method by post-processing the simulation data and results manually. In this section, the entire solution and results are

obtained by using a mathematical optimiser since the design variables are mutually interdependent. The approach is to assume that there must be optima design variables at which the system will perform best. A numerical algorithm, Dynamic-Q [30], is employed and incorporated into the finite volume solver and grid (geometry and mesh) generation package, as shown in Fig. 4, to search and identify the optimal design variables at which the system will perform optimally for more efficient and better accuracy. The algorithm is also specifically designed to handle constraint problems where the objective and constraint functions are expensive to evaluate.

The mathematical optimisation algorithm is a multidimensional and robust gradient-based optimisation algorithm which does not require an explicit line search. The technique involves the application of a dynamic trajectory LFOPC (leapfrog optimisation program for constrained problems) which is adapted to handle constrained problems through approximate penalty function formulations [31]. This dynamic approach is applied to successive approximate quadratic sub-problems of the original problem. The successive sub-problems are constructed from sampling, at relative high
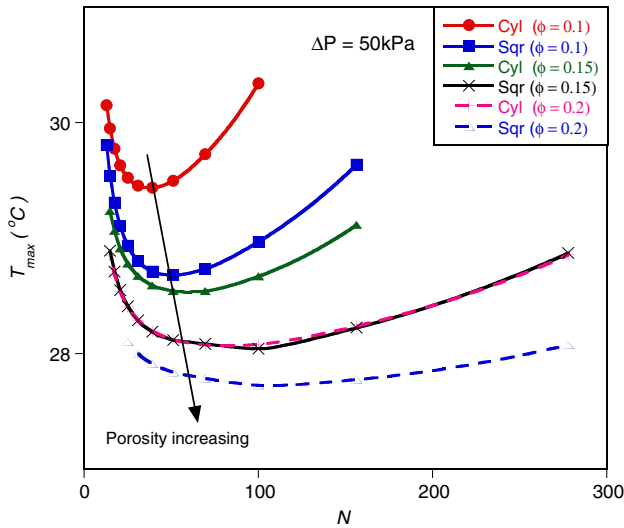
Fig. 10. Effect of optimised total number of channels, N, on the peak temperature.

Fig. 11. Objective function history for cylindrical configuration.

computational expense, the behaviour of the objective function at successive approximate solution points in the design space. The sub-problems, which are analytically simple, are solved quickly and economically using the adapted dynamic trajectory method. The details of the Dynamic-Q and application can be found in open literature [32–34].

6. Optimal configurations using the mathematical optimisation

The optimisation technique described above was been applied to the models described in Section 2. This technique can also be used it as future tool in solving problems involving the constructal theory and optimisation.

6.1. Optimisation problem and design variable constraints

The constraint ranges for the optimisation are:

$$0.1 \leqslant \phi \leqslant 0.2 \tag{21}$$

$$0.025 \text{ mm}^3 \leqslant v_{el} \leqslant 5 \text{ mm}^3 \tag{22}$$

$$0 \leqslant d_h \leqslant w \tag{23}$$

and

$$0 \leqslant s \leqslant w \tag{24}$$

The design and optimisation technique involve the search for and identification of the channel layout that minimises the peak temperature, T_{max}, such that the minimum thermal resistance between the fixed volume and the cooling fluid is obtained with the desired objectives function. The hydraulic diameter and the channel spacing and elemental volume were considered as design variables for the two configurations in the study. A number of numerical optimisations and calculations were carried out within the design constraint ranges given in Eqs. (21)-(24) and the results are presented in the succeeding section in order to show the optimal behaviour of the entire system. The elemental volume of the structure was in the range of 0.025 mm³ to 5 mm³. The optimisation process was repeated for pressure differences across the axial length ranging from 5 kPa to 50 kPa.

Fig. 11 shows the optimisation search history of the objective function with respect to iteration for cylindrical configuration in the optimisation searching process by the mathematical optimiser.
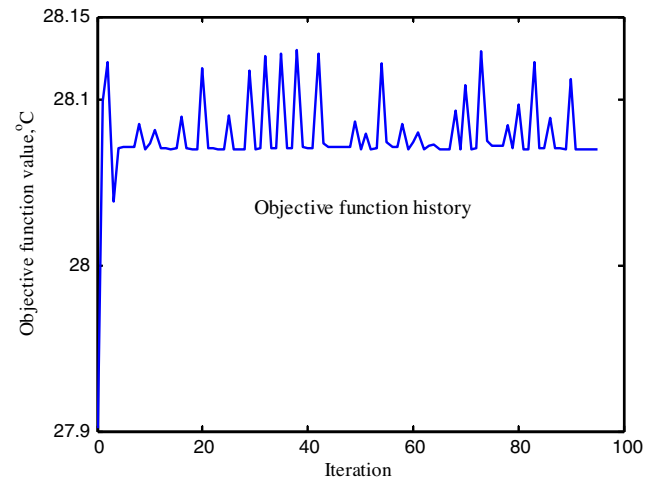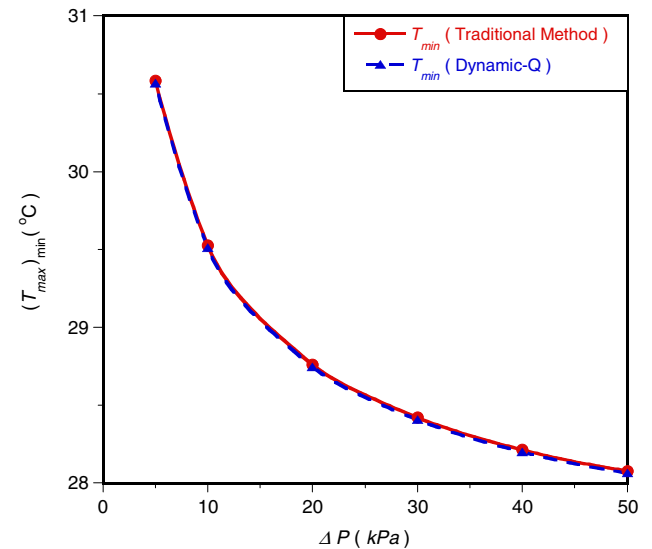
Fig. 12. Comparison of the minimised temperature curve between the traditional method and optimised cylindrical configuration.

Figs. 12 and 13 compare the performance of the cooling channel between the traditional method and mathematical optimiser. Fig. 12 shows minimised peak temperature curves as a function of pressure drop between the traditional method and the optimiser. The optimised result has a slightly better performance than that of the traditional method. This is due to the fact that the optimiser uses a very small step size of the design variables to accomplish the task. Fig. 13 shows the optimised hydraulic diameter curves. The optimised hydraulic diameter decreases as the pressure difference increases, and the optimised hydraulic diameter is smaller in the optimisation process than in the traditional method. In the case of the traditional method, it shows that when the pressure difference is beyond 30 kPa, the pressure difference has no effect on the optimised hydraulic diameter. Whereas, the optimisation tool shows that pressure difference slightly influences the optimised shape.

6.2. Effect of applied pressure difference on optimised geometry and peak temperature

Fig. 14 shows the minimised peak temperature at different porosities for the two configurations. The minimised peak
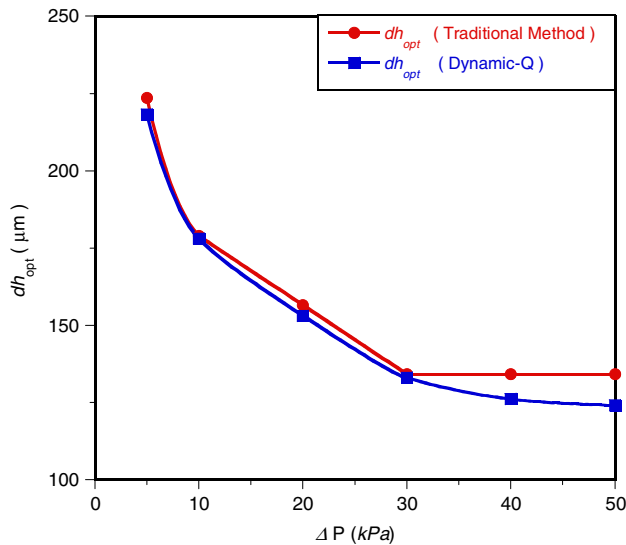
Fig. 13. Comparison of the optimised design variable curves between the traditional method and optimised for cylindrical configuration.

temperature decreases as the pressure difference across the axial length increases for different porosity arrangements. As the pressure difference and porosity keep increasing, the peak temperature becomes less sensitive. The trend is in agreement with previous works [35].

The optimal behaviours of the circular and square configurations with respect to applied pressure difference are reported in Figs. 15 and 17. Fig. 15 shows that there is an optimal unit volume for each of the two configurations. It also shows that the optimised global elemental volume decreases as the pressure difference increases and this lies in the region of 0.5 mm³ ≤ v_{el} ≤ 2.4 mm³. This again, shows that the optimal arrangement of the elemental volume for the entire structure should be very small to achieve better cooling. In Fig. 16, the global $d_{h_{opt}}$ and s_{opt} decrease as the pressure difference increases. $d_{h_{opt}}$ and s_{opt} lie in the vicinity of 100 μm ≤ d_h ≤ 270 μm. It is also observed that the s_{opt} deceases as the $d_{h_{opt}}$ decreases, this is due to the fact that the elemental volume is not fixed for a fixed porosity and there is no optimum porosity. Fig. 17, shows total number of channels arrangement is a function of pressure differ-

Fig. 15. The effect of pressure difference on optimised elemental volume.
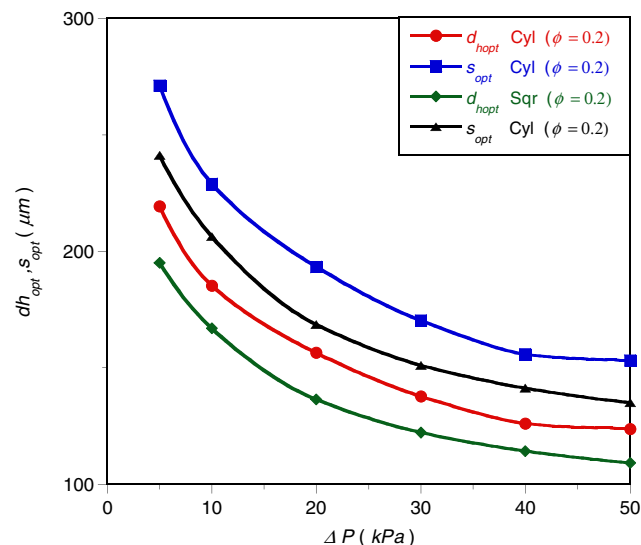
Fig. 16. The effect of pressure difference on optimised hydraulic diameter and optimised spacing.

ence and porosity increases. The global N_{opt} increases as the pressure difference and porosity increase. N_{opt} lies in the region of 10 ≤ N_{opt} ≤ 100. It is also, observed that there is a unique optimal number of channels for every diving force (ΔP) required for each configuration to achieve effective cooling.

7. Method of intersection of asymptotes for conjugate channels with internal heat generation

This section deals with a theoretical analysis which is presented for the circular and square configurations using the intersection of asymptotes method to provide the existence of an optimal geometry, which minimises the global thermal resistance. The following assumptions are made throughout the analysis: the inlet temperature and the pressure difference, ΔP, are fixed with a uniform flow distribution in all the channels, laminar flow, constant cross-sectional area of the channels, negligible inlet and exit plenum losses, and negligible axial conduction. An elemental volume is considered because of the symmetry of the heat distribution.
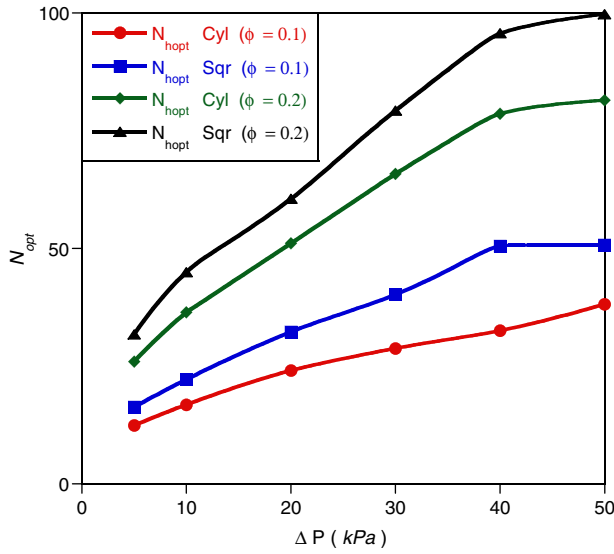

Fig. 14. The effect of pressure difference and porosity on optimised peak temperature.

Fig. 17. The effect of pressure difference on optimised total number of channels.

The heat generated in the elemental volume [12,15] is:

$$\dot{q} = q'''(A_s - A_c)L \tag{25}$$

The heat is conducted and is deposited as the heat flux, q'', through the solid wall to the fluid, therefore,

$$q'''(A_s - A_c)L = q''P_cL \tag{26}$$

The porosity is assumed to be fixed $\varphi = A_c/A_s$, therefore Eq. (26) becomes

$$q'' = \frac{1}{4}q'''_h\beta \tag{27}$$

where β is the numerical value determined from the porosity of the channel and is defined as:

$$\beta = \left(\frac{1-\phi}{\phi}\right) \tag{28}$$

And d_h is the channel hydraulic diameter defined as:

$$d_h = \frac{4A_c}{P_c} \tag{29}$$

The global thermal resistance or global thermal conductance will be determined in two extreme limits.

7.1. Extreme limit 1: small channel

When the channel's characteristic dimension is very small and very slender, that is $d_h \rightarrow 0$ and $d_h \ll L$, the flow is fully developed along the length, L. From the first law of thermodynamics, the rate of heat transfer in a unit volume to the working fluid is equal to enthalpy gained by the working fluid, and then for constant, Cp

$$\dot{q}_s = \rho A_c \bar{u} C_p (T_{out} - T_{in}) \tag{30}$$

In this extreme limit, the fluid in the channel quickly becomes fully developed flow and the working fluid is overworked in such a way that the outlet temperature T_{out} approaches the peak temperature, T_{max}, at the solid structure.

Therefore, Eq. (30) becomes,

$$\dot{q}_{sm} = \rho A_c \bar{u} C_p (T_{max} - T_{in}) \tag{31}$$

This is equal to the heat deposited as heat flux, q'', through the wall to the fluid, therefore

$$\rho A_c \bar{u} C_p (T_{max} - T_{in}) = q''P_cL \tag{32}$$

The average velocity, $\bar{u}$, when the flow is fully developed is given by Hagen–Poiseuille as:

$$\bar{u} = \frac{\Delta P \varsigma^2}{4\mu P_{o_\varsigma} L} \tag{33}$$

where ζ is the characteristic dimension used to define the Poiseuille number, P_o, and in this case the hydraulic diameter, d_h.

Combine Eqs. (32) and (33) and substitute ζ as d_h, then rearrange to get

$$(T_{max} - T_{in}) = q'' \left(\frac{16\mu P_{o_{d_h}}L^2}{\rho d_h^3 C_p \Delta P}\right) \tag{34}$$

Substituting Eq. (27) into Eq. (34) and rearrange to get,

$$\frac{(T_{max} - T_{in})}{q'''L^2} = \beta \left(\frac{4\mu P_{o_{d_h}}}{\rho d_h^2 C_p \Delta P}\right) \tag{35}$$

But,

$$C_p = \frac{k_f \mathrm{Pr}}{\rho v} \tag{36}$$

Substituting Eq. (36) into Eq. (35) and rearranged as:

$$\frac{k_f(T_w - T_{in})}{q'''L^2} = \beta \left(\frac{4\mu v P_{o_{d_h}}}{d_h^2 \mathrm{Pr}\Delta P}\right) \tag{37}$$

The dimensionless global thermal resistance is defined in terms of dimensionless pressure difference as:

$$R = \left[\frac{k_f(T_{max} - T_{in})}{q'''L^2}\right] \cong 4P_{o_{d_h}}\beta\left(\frac{d_h}{L}\right)^{-2}Be^{-1} \tag{38}$$

where

$$Be = \frac{\Delta PL^2}{\mu\alpha} \tag{39}$$

From Eq. (38) for a smaller channel $d_h \ll L$, the thermal resistance is inversely proportional to d_h^2. Keeping β (which is a function of porosity) constant, it shows that the global thermal resistance increases as the hydraulic diameter decreases.

7.2. Extreme limit 2: large channel

In this extreme limit, the channel's characteristic dimension is sufficiently large. That is $d_h \rightarrow \infty$, the boundary layer of surface becomes distinct and the channel diameter is larger than the boundary layer thickness. The working fluid is not properly utilised and working fluid outside the boundary layers becomes useless and the body is not properly cooled in the downstream.

The rate of heat transfer across the thermal boundary layer is

$$\dot{q}_l = hA_s(T_{max} - T_{in}) \tag{40}$$

and the heat flux is

$$\dot{q}''_l = h(T_{max} - T_{in}) \tag{41}$$

The heat transfer rate can be related to Nusselt number and heat transfer coefficient over the unit system. The heat transfer coefficient is defined [36] for a laminar boundary layer as:

$$\frac{hL}{k_f} = 0.453k_f \mathrm{Pr}^{1/3}\mathrm{Re}^{1/2} \quad \text{for } 0.5 < Pr < 10 \tag{42}$$

Substitute Eq. (42) into (41) to get

$$\dot{q}_l'' = \frac{0.453 k_f \text{Pr}^{1/3} \text{Re}^{1/2}}{L}(T_{max} - T_{in}) \qquad (43)$$

where

$$\text{Re}_L = \frac{\bar{u}_\infty L}{v} \qquad (44)$$

u_∞ is the free-stream velocity that sweeps the boundary layers, but the longitudinal pressure force balance on the control volume inscribed inside a unit volume channel is

$$\Delta P A_c = P_c L \bar{\tau}_w \qquad (45)$$

where $\bar{\tau}_w$ is the average wall shear stress over the length and can be obtained from the laminar boundary layer flow solution [36] as:

$$\bar{\tau}_w = 0.664 \rho u_\infty^2 \text{Re}_L^{-1/2} \qquad (46)$$

Combine Eqs. (29) and (44) to Eq. (46) to obtain

$$Re_L = \left(\frac{\Delta P d_h L}{2.656 \rho v^2}\right)^{2/3} \qquad (47)$$

Substitute Eq. (47) into Eq. (43) to obtain

$$\dot{q}_l'' = \frac{0.3271 k_f \text{Pr}^{1/3}}{L}\left(\frac{\Delta P d_h L}{\rho v^2}\right)^{1/3}(T_{max} - T_{in}) \qquad (48)$$

Substitute Eq. (27) into Eq. (48) and rearrange to define the dimensionless global thermal resistance as:

$$R = \left[\frac{k_f(T_{max} - T_{in})}{q'''L^2}\right] \cong 0.7643 \beta \left(\frac{d_h}{L}\right)^{2/3} Be^{-1/3} \qquad (49)$$

From Eq. (49), for a larger channel, the global thermal resistance is directly proportional to $d_h^{2/3}$. Keeping β (which is a function of porosity) constant, confirms that as the hydraulic diameter becomes lager, the global thermal resistance increases.

The geometric optimisation in terms of channel could be achieved by combining Eqs. (38) and (49) using the intersection of asymptotes method as shown in Fig. 18. The optimal dimension can be generally approximated for the two configurations as hydraulic diameter where the two extreme curves intersect. The intersection result is:

$$\left(\frac{d_h}{L}\right)_{opt} \approx 1.8602 P_{o_{d_h}}^{3/8} Be^{-1/4} \qquad (50)$$

where $d_{h_{opt}}$ is the optimal hydraulic diameter and for circular channel $P_{o_{d_h}} = 8$, hence Eq. (50) reduces to
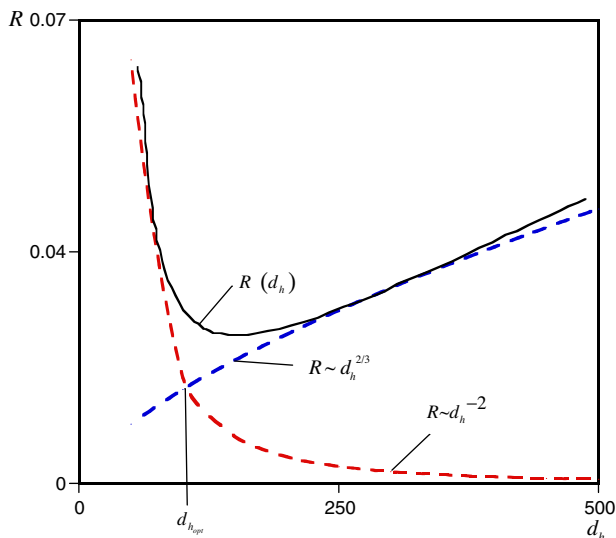

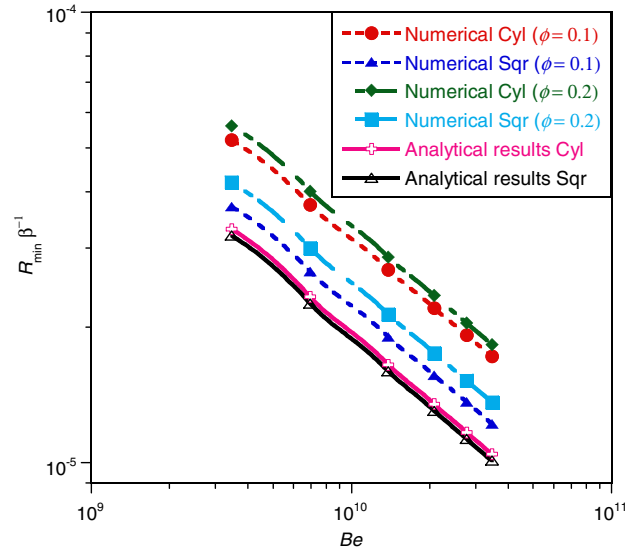**Fig. 18.** Method of intersection of asymptotes: Global thermal resistance.

Fig. 19. Effect of dimensionless pressure difference on the dimensionless global thermal resistance.

$$\left(\frac{d_h}{L}\right)_{opt} \approx 4.057 Be^{-1/4} \qquad (51)$$

For a square channel with hydraulic diameter d_h, $P_{o_{d_h}} = 7$, and hence Eq. (50) reduces to:

$$\left(\frac{d_h}{L}\right)_{opt} \approx 3.859 Be^{-1/4} \qquad (52)$$

The optimal spacing s_{opt} follows from Eqs. (3), (6), and (50):

$$\left(\frac{s}{L}\right)_{opt} \approx 1.8602[(1 + \beta)^{1/2} - 1]P_{o_{d_h}}^{3/8} Be^{-1/4} \qquad (53)$$

Eqs. (50) and (53) show that in the two extremes, the hydraulic diameter and channel spacing decreases as the pressure difference increases for fixed porosity.

The minimum dimensionless global thermal resistance can be obtained for an elemental volume for the two configurations that
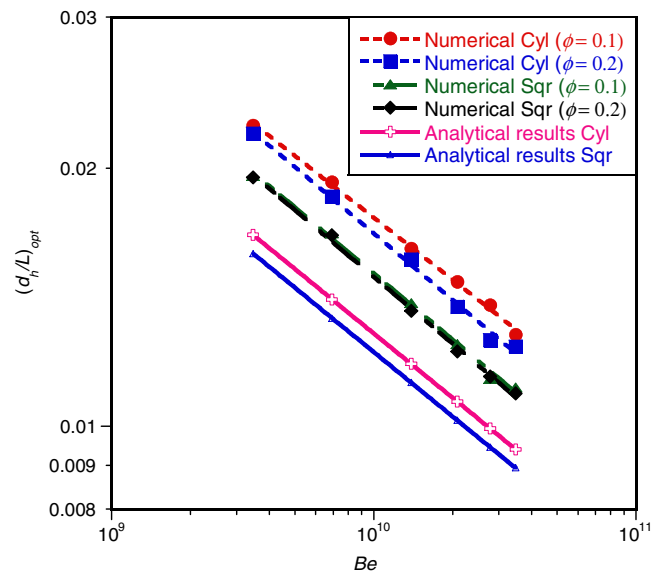

Fig. 20. The effect of dimensionless pressure difference on the optimised hydraulic diameter.
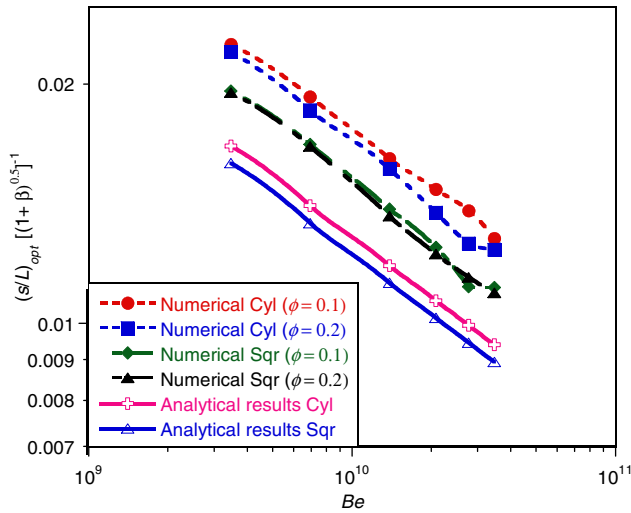
Fig. 21. The effect of dimensionless pressure difference on optimised spacing.

correspond to the optimal geometries by substituting Eq. (50) into Eq. (38) as:

$$R_{\min} = 1.156\beta P_{o_{d_h}}^{1/4} Be^{-1/2} \tag{54}$$

Eq. (54) shows that the thermal resistance decreases monotonically as Be increases for a fixed porosity.

The minimised dimensionless global thermal resistance of a circular channel with $P_{o_{d_h}} = 8$ is:

$$R_{\min} = 1.9442\beta Be^{-1/2} \tag{55}$$

and the minimised dimensionless global thermal resistance of a square channel with $P_{o_{d_h}} = 7$ is:

$$R_{\min} = 1.8803\beta Be^{-1/2} \tag{56}$$

8. Comparison of the theoretical method and numerical optimisation

8.1. The effect of dimensionless pressure difference on the minimised dimensionless global thermal resistance

Fig. 19 shows the minimised dimensionless global thermal resistance as a function of dimensionless pressure difference at optimised design variables for the two configurations. The analytical results of Eqs. (55) and (56) validate the numerical solutions. The two optimised solutions have similar trends. Also, the analytical results and the numerical results show that in the two optimised configurations, the minimised global thermal resistance decreases as the dimensionless pressure difference increases. Although the analytical results are lower than numerical results, the theoretical and numerical values agree within a factor of 1.8 for the worst case. These results are also in agreement with past research work [12,15,35].

Eqs. (57) and (58) are the correlations for minimised dimensionless thermal resistance and the dimensionless pressure difference for cylindrical and square channels, which are obtained when the cooling geometry is optimised in order to achieve cooling for $\varphi = 0.2$

$$R_{\min,Cyl} = 9.64Be^{-0.49} \tag{57}$$

And

$$R_{\min,Sqr} = 7.68Be^{-0.49} \tag{58}$$

8.2. Effect of applied dimensionless pressure difference on optimised design variables

Figs. 20 and 21 show the effect of the dimensionless pressure difference on the optimised design variable for circular and square configurations. The curves show that design variables decrease as applied dimensionless pressure difference and porosity increase. Also the optimised spacing is directly proportional to the optimised hydraulic diameter. This is also due to the fact that the elemental volume is not fixed, but it is allowed to morph for a fixed porosity. This shows that unique optimal design geometries exist for each applied dimensionless pressure number for each configuration.

Fig. 22a and b show the temperature contours of the elemental structure for circular and square configurations, respectively. Fig. 20c and d show the temperature contours of the inner wall of the cooling channel with cooling fluid for circular and square configurations, respectively. The blue region indicates the region of low temperature and the red region indicates that of high temperature.
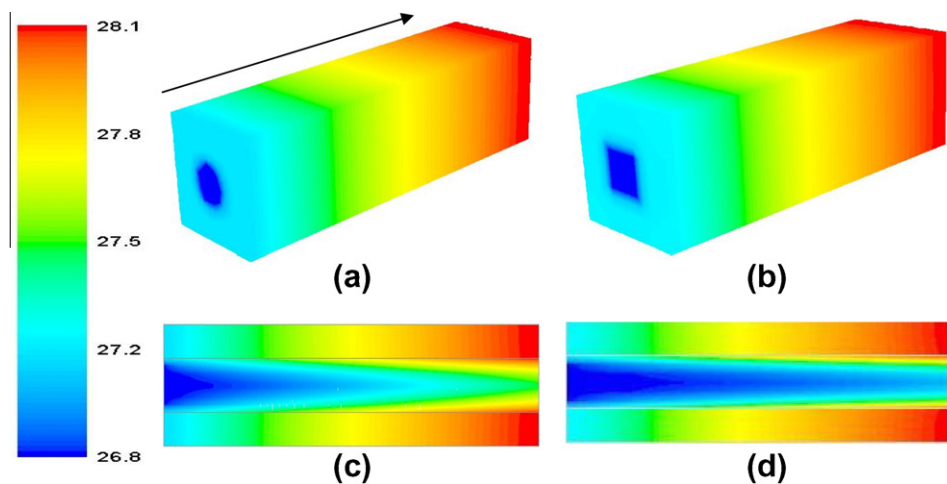

Fig. 22. Temperature distributions on the cooling fluid and inner wall, and unit structure.

9. Conclusion

This paper studied the numerical and analytical optimisation of geometric structures of cooling volumes with internal heat generation for cylindrical and square channel cross-sections. The results showed that there is an optimal geometry for the two channel configurations considered, which minimises the peak temperature and hence thermal resistance. The numerical analysis also showed that the global optimal hydraulic diameter and channel spacing decrease as the pressure difference increases for fixed global volume constraint due to the fact that the elemental volume is not fixed, but allowed to morph for a fixed porosity. This shows the existence of unique optimal design variables (geometries) for a given applied dimensionless pressure number for each configuration. The results also show that the minimised peak temperature decreases as the porosity increases. It is also observed that the optimal total number of channels is a function of pressure difference. From the result, it is also observed that the square channel has better performance than the cylindrical channel.

The numerical results obtained are in good agreement with results obtained in the approximate solutions based on scale analysis at optimal geometry dimensions. The approximate dimensionless global thermal resistance predicts the trend obtained in the numerical results. The use of the optimisation algorithm coupled to the CFD package made the numerical results to be more robust with respect to the selection of optima structures' geometries, internal configurations of the flow channels, total number of the channels and dimensionless pressure difference. Future work may consider the optimisation of additional microchannels placed in the interstitial regions of a circular or square tube array for multi-scale design.

Acknowledgements

References

[1] A. Bejan, Advanced Engineering Thermodynamics, second ed., Wiley, New York, 1997.

[2] A. Bejan, E. Sciubba, The optimal spacing of parallel plates cooled by forced convection, Int. J. Heat Mass Transfer 35 (1992) 3259–3264.

[3] A. Bejan, S. Lorente, Design with Constructal Theory, Hoboken Wiley, 2008.

[4] A.H. Reis, Constructal theory: from engineering to physics and how flow systems develop shape and structure, Appl. Mech. Rev. 59 (2006) 269–282.

[5] Y. Fan, L. Luo, Recent Applications of advances in microchannel heat exchangers and multi-scale design optimisation, Heat Transfer Eng. 29 (2008) 461–474.

[6] A. Yilmaz, O. Buyukalaca, T. Yilmaz, Optimum shape and dimensions of ducts for convective heat transfer in laminar flow at constant wall temperature, Int. J. Heat Mass Transfer 43 (2000) 767–775.

[7] Y.S. Muzychka, Constructal design of forced convection cooled micro-channel heat sinks and exchangers, Int. J. Heat Mass Transfer 48 (2005) 3119–3124.

[8] Y.S. Muzychka, Constructal multi-scale design of compact micro-tube heat sinks and heat exchangers, Int J. Therm. Sci. 46 (2007) 245–252.

[9] A.K. da Silva, S. Lorente, A. Bejan, Optimal distribution of discrete heat sources on a plate with laminar forced convection, Int. Int. J. Heat Mass Transfer 47 (2004) 2139–2148.

[10] A. Bejan, Y. Fautrelle, Constructal multi-scale structure for maximal heat transfer density, Acta Mech. 163 (2003) 39–49.

[11] T. Bello-Ochende, A. Bejan, Maximum heat transfer density: Plates with multiple lengths in forced convection, Int. J. Therm. Sci. 43 (2004) 1181–1186.

[12] T. Bello-Ochende, L. Liebenberg, J.P. Meyer, A.G. Malan, A. Bejan, J.P. Meyer, Constructal conjugate heat transfer in three-dimensional cooling channels, Int. J. Heat Mass Transfer 14 (2007) 279–293.

[13] T. Bello-Ochende, L. Liebenberg, J.P. Meyer, Constructal cooling channels for micro-channel heat sinks, Int. J. Heat Mass Transfer 50 (2007) 4141–4150.

[14] R.S. Matos, J.V.C. Vargas, A. Bejan, Three-dimensional optimization of staggered finned circular and elliptic tubes in forced convection, Int. J. Heat Mass Transfer 44 (2000) 3953–3961.

[15] J.C. Ordonez, Integrative energy-systems design: system structure from thermodynamic optimization, Ph.D. thesis Duke University USA, 2003.

[16] A.H. Reis, A.F. Miguel, A. Bejan, Constructal Theory of particle agglomeration of design of air-cleaning devices, J. Phys. D: Appl. Phys. 39 (2006) 3086–3096.

[17] Y. Kim, S. Lorente, A. Bejan, Steam generator structure: continuous model and constructal design, Int. J. Energy Res. 35 (2011) 336–345.

[18] G. Lorenzini, C. Biserni, L.A.O. Rocha, Geometric optimization of isothermal cavities according to Bejan's theory, Int. J. Heat Mass Transfer 54 (2011) 3868–3873.

[19] L.A.O. Rocha, E. Lorenzini, C. Biserni, Y. Cho, Constructal design of a cavity cooled by convection, Int. J. Des. Ecodyn. 5 (2010) 212–220.

[20] H.H. Bau, Optimization of conduit shapes in micro heat exchangers Int, J. Heat Mass Transfer 41 (1998) 2717–2723.

[21] R.C. Chu, Thermal management roadmap cooling electronic products from hand held device to supercomputers, in: Proceedings of MIT Rohsenow Symposium Cambridge, MA, 2002.

[22] SEMATECH The National Technology Roadmap For Semiconductors: Technology Need SEMATECH, Austin, TX, 1997.

[23] S. Bhattacharjee, W.L. Grosshandler, The formation of wall jet near a high temperature wall under microgravity environment, ASME HTD 96 (1988) 711–716.

[24] S. Petrescu, Comments on the optimal spacing of parallel plates cooled by forced convection, Int. J. Heat Mass Transfer 37 (1994) 1283.

[25] Fluent Inc., Fluent Version 6 Manuals, Centerra Resource Park, 10 Cavendish Court, Lebanon, New Hampshire, USA, 2001 (www.fluent.com).

[26] S.V. Patankar, Numerical Heat Transfer and Fluid flow, Hemisphere, New York, 1980.

[27] Fluent Inc., Gambit Version 6 Manuals, Centerra Resource Park, 10 Cavendish Court, Lebanon, New Hampshire, USA, 2001 (www.fluent.com).

[28] The MathWorks, Inc., MATLAB & Simulink Release Notes for R2008a, 3 Apple Hill Drive, Natick, MA, 2008 (www.mathworks.com).

[29] F.M. White, Viscous Fluid Flow, 2nd ed., McGraw-Hill International Editions, Singapore, 1991.

[30] J.A. Snyman, A.M. Hay, The DYNAMIC-Q Optimization Method: An alternative to SQP?, Comput Math. Appl. 44 (2002) 1589–1598.

[31] J.A. Snyman, N. Stander, W.J. Roux, Dynamic penalty function method for the solution of structural optimization problems, Appl. Math. Model. 18 (1994) 453–460.

[32] J.A. Visser, D.J. de Kock, Optimization of heat sink mass using the DYNAMIC-Q numerical optimization method, Commun. Numer. Meth. Eng. 18 (2002) 721–727.

[33] T. Bello-Ochende, J.P. Meyer, F.U. Ighalo, Combined numerical optimization and constructal theory for the design of Microchannel heat sinks, Numer. Heat Transfer A 58 (2010) 882–899.

[34] O.T. Olakoyejo, T. Bello-Ochende, J.P. Meyer, Mathematical optimisation of laminar forced convection heat transfer through a vascularised solid with square channels, Int. J. Heat Mass Transfer 55 (2012) 2402–2411.

[35] O.T. Olakoyejo, T. Bello-Ochende, J.P. Meyer, Geometric optimisation of forced convection in cooling channels with internal heat generation, in: Proceedings of the 14th International Heat Transfer Conference, Washington DC, USA, 2010.

[36] A. Bejan, Convection Heat Transfer, third ed., Wiley, Hoboken, 2004.